NASA CR- 143678

ANALYTICAL SYSTEMS ENGINEERING CORPORATION

Dr. R. G. Stone
Code 693
1-27-75

GODDARD SPACE FLIGHT CENTER

REQUEST FOR APPROVAL FOR PUBLICATION AND RELEASE

A-3047

(See Reverse for Detailed Instructions) (Refer to GHB 2220.8, Approval and Special Requirements for GSFC Publications)

NASA CR 143678

1. X—Document Number ASCR 73-52 NAS 5-23224	2. Title Thunderstorms Observed by Radio Astronomy Explorer I Over Regions of Low Man Made Noise Final Report
ALL COSTS TO BE CHARGED TO	
3. GSFC job order number	Typed name and signature of Author(s) Joseph A. Caruso & John R. Herman
NASA agency-wide code designation	Analytical Systems Engineering Corporation, Burlington, MA
4. APPROVAL REQUESTED AS ☐ Presentation ☐ Working Paper ☐ Journal Publication ☐ Preprint ☐ Formal NASA Report ☐ Thesis ☐ CR Publication ☐ CR Release	dated May 1974 Article I Para. A NAS 5-23224 (March 13, 1973 - March 13, 1974)

NOTE: COMPLETE FOR PRESENTATIONS, JOURNAL PUBLICATION AND PREPRINTS

5. Name of organization or professional meeting, location and date held	6. Name of journal, proceedings, etc.

DOES	DOES NOT	7. PUBLICATION CONTENT CONSIDERATIONS:
☐	☒	Contain Classified Material
☐	☒	Use International System of Units (SI)
☐*	☒	Describe Potentially Patentable Subject Matter (I.E., A new and useful process, product, mechanical and electrical arrangement of parts, or composition or matter.)

*Forward to Patent Counsel, Code 204

7a. Typed name and signature of reviewer in Office of Patent Counsel

8. This paper has been prepared keeping specifically in mind trade secrets or suggestions of outside individuals or concerns which have been communicated to the Center in confidence, and does not violate any such disclosures, and has been examined to see that all participating groups have been given proper credit.

Primary Author

APPROVALS AND APPROVAL AUTHORITY (See instructions on the reverse of this form)

		Comments	Code	Date
9a. Typed name and signature of Branch Head	☒ Approve ☐ Disapprove			
b. Typed name and signature of Division Chief N.F. NESS	☒ Approve ☐ Disapprove		640	1/28
c. Typed name and signature of Director of	☐ Approve ☐ Disapprove			
d. Typed name and signature Office of the Director	☐ Approve ☐ Disclaimer Waived ☐ Disapprove			

MAR 1975 RECEIVED NASA STI FACILITY INPUT BRANCH

DOCUMENT RELEASE INSTRUCTIONS

10.

A. PREPRINTS & CONTRACT REPORTS ONLY

☒ Announce in STAR (no limitations on availability) ☐ Release by Originating Office Only

B. WORKING PAPERS (Operational Documents) & CONTRACT REPORTS

1. Announce in CSTAR (distribution limited as indicated) 2. ☐ Release by Originating Office Only
   - a. ☐ U. S. Government Agencies and Contractors Only
   - b. ☐ U. S. Government Agencies Only
   - c. ☐ NASA and NASA contractors Only

11. **PRINTING SPECIFICATIONS (X-Documents Only)**

Normal printing includes the use of a standard 8 x 10½ cover, pages printed on both sides, with binding accomplished using two staples in the left margin.

Requester's Name					Job Order Number		
Code	Bldg.	Room	Phone	Date of Request	Date Required	No. of Originals	No. of Copies

GSFC 25-42 (8/74)

1 — PRINTING AND DUPLICATING SECTION

INSTRUCTIONS FOR COMPLETING FORM

BLOCK	INSTRUCTIONS
1	Enter X-Document number; Preprints and working papers are published as X-Documents. The document number assignments and covers are issued by the Production Section, Publications Branch.
2	Type in the publication title and authors name(s). (Some working papers will have no author identified.)
3	GSFC Job Order No. = TID support job order NASA Agency-wide code = Unique Project Number (UPN)
4	Check type of publication. If preprint is checked so must final publication be checked.
5	Complete if a presentation. Approval will not be made if not completed.
6	Complete if journal article. Approval will not be made if not completed.
7	Check as applicable.
7a	Required if report describes potentially patentable subject matter.
8	Signed by primary author.
9	Approval Requirements as follows: a. Branch Head: All publications (if approval is for reprinting, without change, of an X-Document this should be indicated). b. Division Chief: All publications, except reprintings of X-Documents – THIS REQUIREMENT IS NON-DELEGABLE. c. Directors of: Presentations, journal articles, formal NASA reports and preprints – Approval for the preparation of preprints MAY be delegated with the concurrence of the Office of the Director. d. Office of the Director: (See NASA Management Delegation 2220.7.) (1) If the information is contained in or extracted from an advanced study report or was obtained as a result of an in-house or contracted advanced study. In this sense, an advanced study is one that can be interpreted as the Agency's position or intent regarding a new system or mission beyond those currently approved. (2) If the information is to be presented at, or published in the proceedings of any meeting (regardless of location) sponsored by a foreign or international organization, or will be submitted to international organizations or foreign governments, individuals or publishers. (See NMD/AD 9710.1B). (3) When it is determined that: (a) The information contains any conflict with previous statements made in testimony, reports or other communications to the Congress, other Government agencies or to the public. (b) Policy concerning release of the information is not clearly delineated. (c) The information borders on matters held as sensitive by other Government agencies. NOTE: Unless specifically waived by the Director, disclaimer notice will be included.
10	Complete as applicable.
11	Complete as applicable (X-Documents only).

Analytical
Systems Engineering CORPORATION

25 RAY AVENUE
BURLINGTON, MASSACHUSETTS 01803
(617) 272-7910

ASCR 73-52

THUNDERSTORMS OBSERVED BY RADIO ASTRONOMY EXPLORER I OVER REGIONS OF LOW MAN MADE NOISE

BY

Joseph A. Caruso & John R. Herman

May 1974

Final Report on: Contract NAS5-23224, Article 1, Paragraph A
Period Covered: March 13, 1973 - March 13, 1974

Prepared For:
NATIONAL AERONAUTICS & SPACE ADMINISTRATION
Goddard Space Flight Center
Greenbelt, Maryland 20771

ABSTRACT

Radio Astronomy Explorer (RAE) I observations of thunderstorms over regions of low man made noise levels are analyzed to assess the satellite's capability for noise source differentiation. The investigation of storms over Australia indicates that RAE can resolve noise generation due to thunderstorms from the general noise background over areas of low man made noise activity.

Noise temperatures observed by RAE over stormy regions are on the average 10DB higher than noise temperatures over the same regions in the absence of thunderstorms. In order to determine the extent of noise contamination due to distant transmitters ($\tilde{}$ 10,000 km distant) comprehensive three dimensional computer ray tracings were generated. The results indicate that generally, distant transmitters contribute negligibly to the total noise power, being 30DB or more below contributions arriving from an area immediately below the satellite.

Table of Contents

1.0 INTRODUCTION

The Radio Astronomer Explorer (RAE) I satellite has over the past two years furnished both new and significant information regarding the noise environment due to terrestrial sources both on Earth's surface and at a 6000km altitude.

In addition to providing a means of examining large scale variations in the spatial and temporal distribution of noise sources. RAE appears to possess the potential for the detection and analysis of thunderstorm activity. Preliminary results of the analysis of thunderstorms occurring over the United States were presented in some detail in the final report under contract NA55-23121.

Very briefly, the results indicate that the high levels of man made noise over the United States tend to make it difficult to resolve the noise contribution of the thunderstorm from the general noise background.

This final report, examines the results of thunderstorm observations over the northern central highlands of Australia where one expects man made noise levels to be considerably lower. It is our contention that if the assessment of the results of the United States thunderstorm observations are correct, it will be possible to more easily differentiate thunderstorm activity from the general noise background over regions of low man made noise.

A final important area of consideration is the application of three-dimensional computer ray tracing techniques to the cases of thunderstorm activity over Minnesota and RAE noise observations over Pretoria, South Africa, both cases having been discussed in the final report on Contract NAS5-23121.

The Australian storms are presented in Section 2, followed by the application of ray tracing techniques presented in Section 3.

The effects of spatial and temporal variations in ionospheric penetration frequency on the observed noise at RAE altitude are considered throughout this report and accounted for quantitatively where possible.

2.0 Individual Thunderstorm Analysis

The determination of RAE's capacity to distinguish between noise emanating from active thunderstorms and the general noise background in the absence of storm activity has been an important facet of the overall investigation of terrestrial radio noise as observed by RAE. A number of individual thunderstorms occurring over the United States have been investigated and reported upon (J. Herman, et al, 1973). However, as a result of the large projected antenna beam from a height of 6000km coupled with the high density of man made noise sources within the United States, energy added by individual thunderstorms although detectable, represents a small perturbation to the general noise background.

In an attempt to eliminate much of the man made noise background two thunderstorms occurring over the northern central highlands of Australia have been investigated in detail. This particular region is relatively free from man made noise sources and interfering transmitters. Hence, the contribution of an individual thunderstorm within the viewing area should be more easily resolved than was the case for the United States.

Before presenting the analytical results of the storm observations over Australia, the theory relating the variation in viewing area, local critical frequency, observing frequency, and RAE antenna parameters to the received noise power will be presented.

2.1 ELEMENTARY THEORY

The formulation of a general theory of the functional relationship between noise power and observing frequency is quite difficult. Nevertheless, with certain simplifying assumptions and a careful choice of RAE location and observation period a relationship is derived which yields results in good agreement with earlier theoretical studies, and perhaps more significantly with experimental observations.

Figure 1 illustrates a simplified view of the relationship between the noise at the ground, the intervening ionosphere and the terrestrial noise at the satellite. It assumes with flat earth geometry that the ground is visible to the satellite at a height over a circular area of radius R, and the noise is uniformly distributed throughout the area. The radius might be fixed by the ionosphere, the antenna area projected to the ground, or the size of the thunderstorm; at present, the ionosphere appears to be the dominant factor.

The power flux density incident at the satellite P_s ($WM^{-2}Hz^{-1}$) is

$$P_s = \frac{K}{A_s} T_s \qquad (1)$$

where K is Boltzmann's constant, A_s it the RAE antenna aperture, and T_s is the equivalent antenna temperature measured by RAE. Similarly, the power flux density radiated by a point source at the ground is:

$$P_g = \frac{KT_g}{A_g} \qquad (2)$$

Assuming that the energy is radiated isotropically into the half-sphere above the ground, the power flux density at a distance D due to the sources in an elemental area of the extended source (Figure 1) will be:

$$dP_s = \frac{PG\ RdRd\theta}{2\pi D^2} \qquad (3)$$

Where $D^2 = R^2 + H^2$ when RAE is vertically above the extended source center.

The total power flux density is at the satellite is, then,

$$P_s = \int_0^R \int_0^{2\pi} \frac{P_g RdRd\theta}{2\pi\ (R^2 + H^2)} \qquad (4)$$

To make the integration tractable, we have considered only cases where the predicted f_0F_2 contours are of a circular nature surrounding the area in question. Under these circumstances, the expression can be integrated directly with the following result:

$$P_s = \tfrac{1}{2} P_g \ln \frac{(R^2 + H^2)}{H^2} \qquad (5)$$

Since the effective antenna area is:

$$A = \frac{\lambda^2 G}{4\pi}$$

Where G is the gain and λ the wavelength, eqs. 1, 2, and 5 combine to form:

$$T_s = \tfrac{1}{2}\, T_g G_s \ln \frac{(R^2 + H^2)}{H^2} \qquad (6)$$

Where T_g is now the temperature which would be measured at the ground with an omni-directional antenna (G_g=1), and G_s is the gain of the RAE antenna.

If ionospheric refraction is neglected and the ionosphere is assumed to have a critical frequency of f_c and a virtual height of 300 Km, the relationship between the ratio of critical to observing frequency (f) and the great circle distance (L) between a point source and the subsatellite point can be shown to be (Herman, et al 1973):

$$\frac{f_c}{f} = \left[1 - \frac{\sin^2 (L/Re)}{1.39 - 1.14 \cos (L/Re)} \right]^{\frac{1}{2}} \qquad (7)$$

Where Re = 6370 Km the earth's radius.

For a spatially constant critical frequency or an ionosphere concentric about the subsatellite point L=R, the effective viewing area can be deduced from a knowledge of the critical frequency distribution.

To summarize the limitations of equation 6; (a) the source temperature is probably not constant over the whole viewing area, so T_g represents the average temperatures that would be measured by placing an omni-directional antenna at a number of locations within the viewing area; (b) because R equals the satellite horizon (~6500 Km) with no ionosphere, the flat earth approximation breaks down when the critical frequency is sufficiently low; (c)

the viewing area is circular only when the critical frequency throughout the viewing area is either constant or concentrically distributed about the subsatellite point.

The events selected for the analysis are within limitations (b) and (c), but the results are necessarily the average ground noise temperature over the whole viewing area.

2.2 RESULTS OF THUNDERSTORM ANALYSIS OVER AUSTRALIA

The basic objective of the analysis is to determine the difference in received noise power as a function of frequency on RAE passes over a given region during and in the absence of thunderstorm activity.

Since in addition to the restrictions imposed by (b) and (c) above, further limitations are imposed by either data being unavailable for a particular period of thunderstorm activity or RAE not passing over the region of thunderstorm activity at the appropriate time, only two storms were available for analysis.

The first of the storms occurred on December 2, 1968 at 0210LT over Alice Springs, Australia located at 24° south latitude and 134° east longitude. The second storm over Charleville, Australia 26° S, 146° E took place on August 21, 1969 at 0900LT.

Figure 2 illustrates the salient features of the December storm. As indicated in the figure, the noise factor F_a in decibels above $288^{\circ}K$ is plotted as a function of frequency for both the storm pass, indicated by the black circles, while the blackened squares and triangles indicate the noise factor measured respectively, over the same location five and ten days later, in the absence of known thunderstorm activity. Additionally, the CCIR predicted noise factor is also plotted as a function of frequency for comparison with the observational data.

The antenna temperatures were averaged over a three minute interval centered about the time of closest approach to the storm location both during the storm and on the control pass to establish

a representative effective temperature, T_s. Considering the ionosphere to be the limiting factor in the size of the viewing area, each frequency sees a different area, the highest frequency covering the largest area. For the December storm the critical frequency was such that 3.93 and 4.7MHz were completely shielded by the ionosphere. This situation prevails during each of the control days where 3.93MHz is shielded on December 12 and both 3.93 and 4.7MHz are below the critical frequency on December 7.

The measured values of f_0F_2 taken at Mundaring, Australia supplemented by the CRPL predicted values of critical frequency determine the viewing area boundary, i.e. R in equation (4). As pointed out earlier only areas which are approximately circular or can be reasonably constrained to circularity were considered. In these cases $R \tilde{\sim} L$ where L is determined from eq. (7). For the December storm the critical frequency distribution and hence the satellite viewing area is nearly circular over a large section of the continent and the elementary theory has been applied in a straight forward manner.

The limiting value of F_0f_2 within the viewing area boundaries on the storm day is 6MHz. This value has been adjusted on the basis of the measured f_0F2 of 5.4MHz at Mundaring, Australia on December 2, 1968 at 0200LT and the CRPL predictions for the same time period.

An examination of figure 2 indicates that the noise factor on the day of the storm is some 10DB higher than the control day noise levels. This seems to bear out the earlier contention that thunderstorm activity can be more easily resolved in regions where man made noise is relatively low.

In this particular case, the control day noise factor distribution is only slightly higher than the CCIR predicted distribution. As will be presently shown, quite the contrary is true for the August storm where there is as much as a 15DB difference in noise level at 6.55MHz.

Figure 3 illustrates the important features of the analysis of the August storm. Again, for the frequencies 6.55 and 9.18MHz, a difference in noise factor of approximately 10db exists between storm and control passes, while the storm temperatures are some 25db higher than the predicted noise temperatures. Hence, there is a substantial difference between observational and predicted noise levels. Since the ionosphere effectively shielded RAE at 3.93MHz and 4.7MHz on the control pass, no comparison can be made between storm and control days. However, on the storm pass, noise factors on 3.93MHz and 4.7MHz are 20db and 15db, respectively, higher than predicted values. Furthermore, the slope of the storm spectrum is positive, comparing favorably with the predicted spectrum slope. It is possible to conjecture that if observations could have been made on the control pass, the slope of the noise spectrum would remain positive and therefore the noise factors on the lower frequencies would be at least somewhat below the storm levels. Any attempt to assign precise values, however, would be purely speculative.

The August storm is complicated by the fact that the critical frequency is not circularly distributed over the region of interest. Consequently, certain assumptions must be invoked, which cloud the analysis. North of the storm location the predicted critical frequency is 9.5MHz, increasing as one goes further in a north easterly direction. In the north westerly direction toward Indonesia and China the critical frequency remains sufficiently low but changes considerably for small azimuth changes. For southerly directions the f_0F2 contours are circular in nature and fulfill the integration criteria of the elementary theory.

To compensate for the lack of complete circularity the limits of integration of equation (4) were adjusted for both θ and R. Since the overall f_0F2 distributions are quite similar on both the control and storm passes, the same adjustments were applied in both cases. Consequently, differences of noise factor between storm and control day remain valid while comparison with predicted noise factors becomes somewhat tenuous. This may very likely account for the fairly large deviations shown in figure 3.

The analysis of thunderstorm activity over northern central Australia, significant for the relatively low man made noise levels which prevail, indicates that severe thunderstorm activity can be more easily resolved here than, for example, over the United States. The two storms investigated show at least a 10db difference in noise factor between storm and control days. Direct comparison with CCIR predicitons in the case of the Charleville storm suffer from the unfavorable f_0F2 distribution which prevailed, necessitating ad hoc changes in the RAE integrated viewing area. In the case of the Alice Springs storm, where the criteria of the elementary theory are satisfied, comparison between observational and predicted noise factors is favorable.

3.0 Trans-Ionospheric Propagation Analysis

To study in detail the question of what fraction of the received noise can be attributed to sources on the ground directly below RAE compared to that penetrating the ionosphere at great distances, it is important to utilize the capabilities of a three dimensional ray tracing program.

Earlier investigations not involving computer ray tracing have shed a great deal of light on this question (NA55-23121). These results very strongly suggest that nearly all of the radiant energy intercepting RAE arrives from an area immediately below the satellite while direct interference from distant transmitters is negligible and can be ignored. This conclusion is based on four factors:

1. Where ground based measurements were available, direct comparison between concurrent RAE and ground based receiver measurements yield excellent correlation (J.Caruso, 1973). This precludes the possibility of energy arriving at the satellite from remote locations after multiple ionospheric reflections, at least for the specific cases investigated.

2. In every case examined (approximately 1000 cases) where RAE was on the day side and therefore shielded by the ionosphere in the localized region immediately below, the noise level simply did not ever exceed the cosmic noise background. This most emphatically indicates that negligible amounts of radiation arrive from transmitters located on the nightside.

3. "Ground break through" as observed by the burst receiver when RAE I crosses over the sunrise-sunset terminator, clearly indicates that the dominant source of energy reaching the satellite comes from the area beneath the satellite. This effect is discussed in greater detail by Herman, et al (1973).

4. Manual raytracing based on techniques formulated by K. Davies (1965) and others reinforce the conclusions expressed above for a limited number of cases.

To further investigate and substantiate these results, the ITSA three-dimentional raytracing program of K. Davies and R.M. Jones (1969) was employed. The program allows the user to specify electron

density profiles on the basis of measured values of electron density at any geographic location in addition to standard ionospheric models such as the Chapman Layer model. The program also has the capability of tracing rays through the ionosphere up to RAE heights and beyond. However, it does not have a "homing" feature; it will not automatically adjust elevation and azimuth angles to search out those specific rays which pass directly through the receiver location. The user must do his own iteration by judicious selections of elevation and azimuth.

Ray traces were computed for a 10,000 KM path between Urumschi, China and St. Cloud, Minnesota in addition to a propagation path from Urumschi to Pretoria, South Africa. These paths were selected since a number of high powered transmitters are located at Urumschi operating within the RAE bandwidth centered at 9.18 MHz and the fact that these paths have been subjected to an extensive earlier investigation. Manual ray tracing over these paths show that very little energy can arrive from distant transmitters either directly or from relatively remote areas after multiple reflections. No direct paths exist and severe losses are incurred for multi-hop paths. As will be revealed shortly, the three dimensional ray tracing has bolstered these results and furnished additional detailed information along the path trajectories.

The electron density profiles used as an input to the program are based on experimental observations and represent average conditions at discrete locations along the path for a specific season and time of day. The profiles for three times of day corresponding to three positions on the path, at the transmitter, mid-path, and sub-satellite point is read into the computer over a range of heights from 60 to 6000 Km. The program linearly interpolates to determine values of electron density at intermediate points along the path.

The D-region profiles are taken from R.W. Knecht (1966) and J. Belrose (1966), and consist of electron density profiles determined by rocket experiment, partial reflections experiments, and cross modulation measurements. The data is selected to represent normal

conditions at an intermediate level in the solar activity cycle.

E and F-region profiles are also taken from Knecht. The F-region profile extends to the F-region peak somewhere in the neighborhood of 350 Km. Above the peak, from 350 Km to 6000 Km the electron density as a function of height is based on measurements made at the Jicamarca radar observatory near Lima, Peru (K. L. Bowles, 1963).

The program has essentially been utilized in the two dimensional mode; that is, the azimuth angle remained fixed. Consequently, off-great circle path propagation between the transmitter and RAE has not been examined. However, in light of the ray tracing results and the earlier investigations alluded to above, off-great circle propagation appears to be insignificant unless a very unique set of conditions prevail.

Figures 5 through 9 illustrate the ray tracing results for the China to Minnesota path. Figure 10 shows the ray paths computed by manual ray tracing for the same path. The thunderstorms in progress over Wisconsin and Minnesota, and the 3-State region of Kansas, Oklahoma, and Nebraska occurred on the night of 15/16 September 1969. RAE passed near these areas heading southwest at about 0420UT (∿2115LT). At the transmitter location daytime ionospheric conditions prevailed, the time being approximately 1000LT. Looking at Figure 4, the daytime electron density profile at the transmitter location indicates an electron density of 9.6×10^5 cm^{-3} at the F-layer maximum. For the case of quasi-longitudinal propagation, the critical frequency can be calculated using the following expression from Davies (1965):

$$N = 1.24 \times 10^4 f_0^2$$

where N is the electron density. The calculated value of f_0F2 using $9.6 \times 10^5 cm^{-3}$ for the electron density is approximately 8.7 MHz. Therefore, we would not expect any ray on frequencies of 8.7 MHz or less to penetrate the ionosphere in the vicinity of the

transmitter. Figures 5 and 6 illustrate these results clearly. The transmitter is located at the far left of the figures. A portion of the Earth's surface between the transmitter and RAE is divided into 100 Km increments from zero to about 10,000 Km, which is the approximate position of the RAE's subsatellite point (RAE height is approximately 6000 Km). Both figures depict ray traces for an observing frequency of 6.55 MHz for the extraordinary ray. Since the extraordinary critical frequency is higher than that of the ordinary ray, a lack of ionospheric penetration displayed by this ray insures that the ordinary ray will likewise be unable to penetrate the layer. In Figure 5 the elevation angle has been varied from 0° to 60° and the figure indicates there are no paths to RAE either directly or after multiple reflections.

Figure 6 displays the raypaths on 6.55 MHz for elevation angles ranging from 70° to 90°. Again, there is no penetration of the F-layer. The ground range extends only 2000 Km for the nine hops specified in this case. It is quite possible that, for the high elevation angles, rays would penetrate the F-layer at some ground range greater than 2000 Km. However, even after the nine hops specified, the loss incurred is sufficiently great to make any energy contributions from the transmitter negligible.

The situation is in general much the same for 9.18 MHz. The results are summarized in Figures 7, 8, and 9. Figure 7 illustrates the extraordinary ray paths for elevation angles from 0° to 60° in 10° increments between Urumschi and St. Cloud where the ray has been curtailed after 9 hops. Notice that the rays penetrate on $6\frac{1}{2}$ and $7\frac{1}{2}$ hops at elevation angles of 30° and 40° respectively. This is in good agreement with the results of the manual ray tracing. From the earlier analysis these multihop paths are more than 30 dB lower than the RAE measured temperatures.

A partial trace of the ordinary ray for the same range of elevation angles is depicted in Figure 8. Many of the ray paths have been cut off after one or two reflections due to a malfunction of the plotter. However, the digital output indicates that the ray paths closely follow the extraordinary rays, penetrating the ionosphere

on 6½ and 7½ hops at slightly steeper elevation angles.

Figure 9 is a more detailed trace of the extraordinary rays over the range of elevation angles for which penetration takes place. Elevation angle has been varied in 1^{o} steps from 35^{o} to 45^{o} for a total of 11 rays each of which penetrate on either the 6½ or 7½ hop.

Again, we would emphasize that large losses are incurred because of the multiple hops and that the rays which do intercept RAE some 10,000 Km down range and at a 6000 Km height are seen by the Vee antenna side lobes, resulting in a further reduction in noise temperature as compared to sources below the satellite veiwed by the main lobe.

On the basis of the content of Figures 5 through 9, it appears clear that the noise temperature measured by RAE while over Minnesota was uncontaminated by either 9.18 or 6.55 MHz transmitter interference emanating from the Urumschi locale. Since as far as it is possible to ascertain this region represents the prime source of transmitter interference on these frequencies, we have concluded that the prime contributors to the RAE measured noise temperature in this case are those sources encompassed by the main antenna beam viewing an area of varying extent immediately below the satellite depending on observing frequency.

The case of a transmitter located on the nightside with RAE on the dayside has been considered in detail and the results are shown in Figures 11 through 18. The transmitter location is again, Urumschi, China with RAE over Pretoria, South Africa at an azimuth of 45^{o}.

Figure 11 illustrates elevation angles ranging from 0^{o} to 90^{o} in 10^{o} increments. As can be seen from the figure, for elevation angles of 20^{o} or greater rays readily penetrate the ionosphere. Since RAE is about 6000 Km above the subsatellite point, some 10,000 Km down range from the transmitter, the penetrating rays are not received by RAE's antenna.

Since the ray at 10^{o} elevation is trapped in the F-layer and has been traced only out to 5000 Km ground range, a series of ray

tracings were computed to ascertain whether the 10° ray or neighboring rays would penetrate the ionosphere further down range and reach the satellite.

The ray paths for elevation angles from 0° to 20° in 2° increments are shown in Figure 12. As can be seen from the figure, the rays are unable to penetrate the ionospheric layer. However, additional information is furnished by this particular trace since rays with elevation angles of approximately 18° become trapped in the F-layer after single ionospheric and ground reflections.

Figure 13 depicts a bundle of rays with elevation angles ranging from 18.2° to 19.8° in $.2^{\circ}$ increments. In the same manner the rays either remain trapped in the layer or are simply reflected without penetration.

The ray at an elevation angle of 18.8° has been traced out to a ground range of 10,000 Km as shown in Figure 14. At a range of approximately 6600 Km, the ray emerges from the ionosphere toward the surface where it is unable to penetrate the ionospheric layer after further reflections. This behavior is representative and typical of the bundle of trapped rays illustrated in the preceeding figure.

One further possibility has been explored and this is the case of a direct path to RAE for take off angles less than, but very close 20°. Figure 15 shows the ray path at an elevation angles of 19.9°. This ray is unable to penetrate the layer. At 19.95° as shown in figure 16 the ray penetrates the layer maximum but is not in the neighborhood of RAE as the ray proceeds outward with very slight refractive effects evident.

Figure 17 depicts the propagation path for two rays at elevation angles of 19.94° and 19.95°, respectively. Again the rays propagate through regions quite remote relative to RAE. It is important to note that the rays propagate over very similar paths both where refractive effects are large near the F-layer maximum and at greater altitudes where the propagation paths are essentially

linear. This enables one to draw valid conclusions concerning, for example, ray paths for elevation angles between 19.94 and 19.95°.

Accordingly, it is reasonable to state that rays between 19.94 and 19.95° will not exhibit any bizarre characteristics. Rather they will closely follow the paths indicated in Figure 17. Similarly, in the case of the trapped modes illustrated earlier, on the basis of the behavior of the ray path at 18.8°, it can be concluded that neighboring rays will behave in analogous fashion.

The propagation characteristics on 6.55 MHz and 3.93 MHz are shown in Figures 18 and 19. As was expected there are no paths either direct or after multiple reflections to RAE.

The more significant results for the Urumschi to Pretoria path with a nighttime ionosphere over Pretoria and the transmitter on the dayside are depicted in Figures 20 and 21. The figures illustrate both the ordinary and extrordinary rays for elevation angles form 0° to 60°. There are no direct paths to RAE, and although paths exist after multiple reflections, the energy arriving at the satellite is negligible due to the severe reflection losses.

The ray tracing results substantiate and reinforce the conclusions drawn from earlier studies in most encouraging fashion. Most significantly, the quite sophisticated Davies and Jones ray tracing program yield results in excellent agreement with manual ray tracing utilized in prior analysis of both the northern China to Minnesota path and the Urumschi to Pretoria path. Consequently, the Davies and Jones program completely validates the contention that the Minnesota storm analysis and the Pretoria comparison with ground based measurements (J. Herman, 1973) are uncontaminated either by direct path interference or multiple hop remote arrival of energy from distant transmitters.

Further, a detailed ray tracing with regard to the case of distant transmitters on the nightside with RAE on the dayside validates the extensive experimental observations of the noise tempera-

ture when the satellite is on the dayside. Observation invariably indicates noise levels equal to or below the cosmic noise background. It is expected that distant transmitters will contribute negligibly and ray tracing confirms this.

4.0 Summary and Conclusions

Results of a more sophisticated investigation of trans-ionospheric propagation between distant transmitters and RAE when over Australia, fully substantiate the contention that energy arriving directly from distant transmitters is inconsequential, contributing only negligibly to the total noise power. Furthermore, for the specific cases studied, energy arriving after multiple reflections from locations outside the viewing area directly below RAE, suffer severe loss and hence do not contribute significantly to the total noise power.

Although the ray tracing investigation has been confined of necessity to a limited number of cases which have been elucidated upon above, it is felt the conclusions drawn have a more general validity. For multiple hop paths in the neighborhood of 10,000 Km, there will always exist large absorption losses due to two or more passes through the D-Region. Additional losses result from scattering and absorption losses due to ground reflections. The multiple hop path losses suffered will generally reduce energy arriving via this mode to negligible amounts.

Direct propagation paths are not an important consideration for observations over Australia which is surrounded by large bodies of water free of man-made noise. In fact, for the range of elevation angles considered, direct paths do not exist. A careful study of the ray traces indicates that, by induction, there would be no direct path for any elevation angle choosen. This is in accord with the large body of observational data which has been studied both for times and locations above, in addition to times and locations reported on under earlier contract (NA55-23121).

In order that a direct path from a distant transmitter be present and also contribute significantly to the total noise power at the satellite, a number of conditions must be satisfied: the transmitter must be relatively high powered; the electron density profile in the neighborhood of the transmitter must be such that rays are able to penetrate; if rays are able to penetrate, very few,

if any will suffer that precise amount of refraction necessary for the rays to intercept the satellite. For this energy to be significant, the maximum power point of the main antenna beam must point in the direction determined by this small range of elevation and azimuth. This condition does not obtain for the given geometry.

Although large energy contributions via direct paths are certainly conceivable and possible, given the rather stringent conditions which must be fulfilled, they are not very probable.

5.0 REFERENCES

1. Herman, J. R., J. A. Caruso, and R. G. Stone, paper presented at annual fall meeting, AGU, San Francisco, California, December, 1972.

2. Herman, J. R., J. A. Caruso, and R. G. Stone, Planetary Space Science, Vol. 21, 1973.

3. Caruso, J. A., and J. R. Herman, Thunderstorms and Groundbased Radio Noise as Observed by Radio Astronomy Explorer I, Final Report, NA55-23121, April, 1973.

4. Caruso, J. A., J. R. Herman, and R. T. Disney, paper presented at fall URSI meeting, Williamsburg, Va., December, 1972.

5. Davies, K., Ionospheric Radio Propagation, U. S. Government Printing Office, 1965.

6. Davies, K. and R. M. Jones, AGARD Conference Proceedings, No. 13, pg. 173-198, 1969.

7. Knecht, R. W., Progress in Radio Science, 1960-1963, pg. 14-45 Ed. G. M. Brown, Elsevier Publishing Co., 1965.

8. Belrose, J. S., L. R. Bode, and L. W. Hewitt, Electron Density Profiles in Ionosphere and Exosphere, Ed. J. Frihagen, North-Holland Publishing, Co., 1966.

9. Bowles, K. L. Science, Vol. 139, No. 3553, February, 1963.

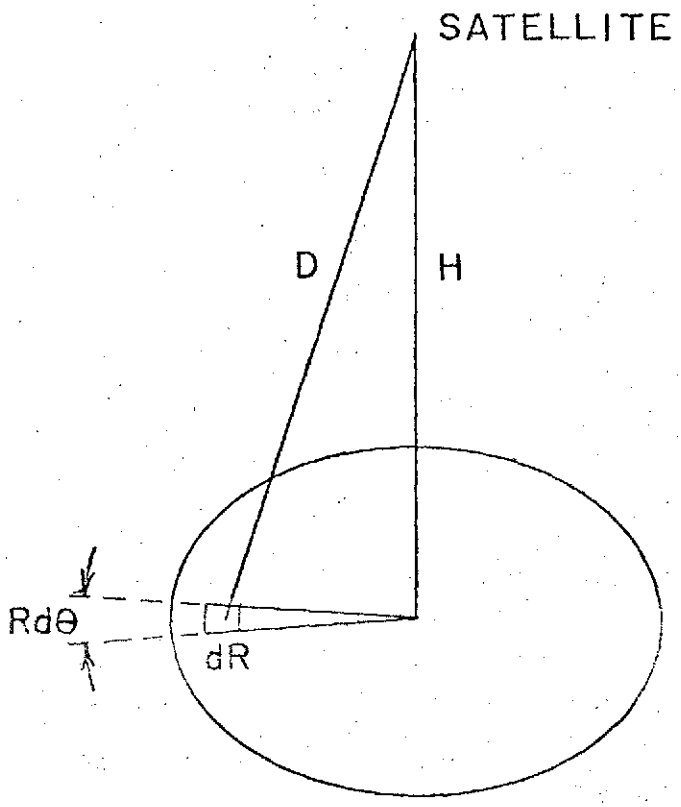

$$dP_s = \frac{P_g}{2\pi D^2} R\,d\theta\,dR$$

$$D^2 = R^2 + H^2$$

$$P_s = \tfrac{1}{2} P_g \ln\left(\frac{R^2 + H^2}{H^2}\right)$$

$$T_s = \tfrac{1}{2} T_g G_s \ln\left(\frac{R^2 \quad H^2}{H^2}\right)$$

FIGURE 1

FIGURE 2

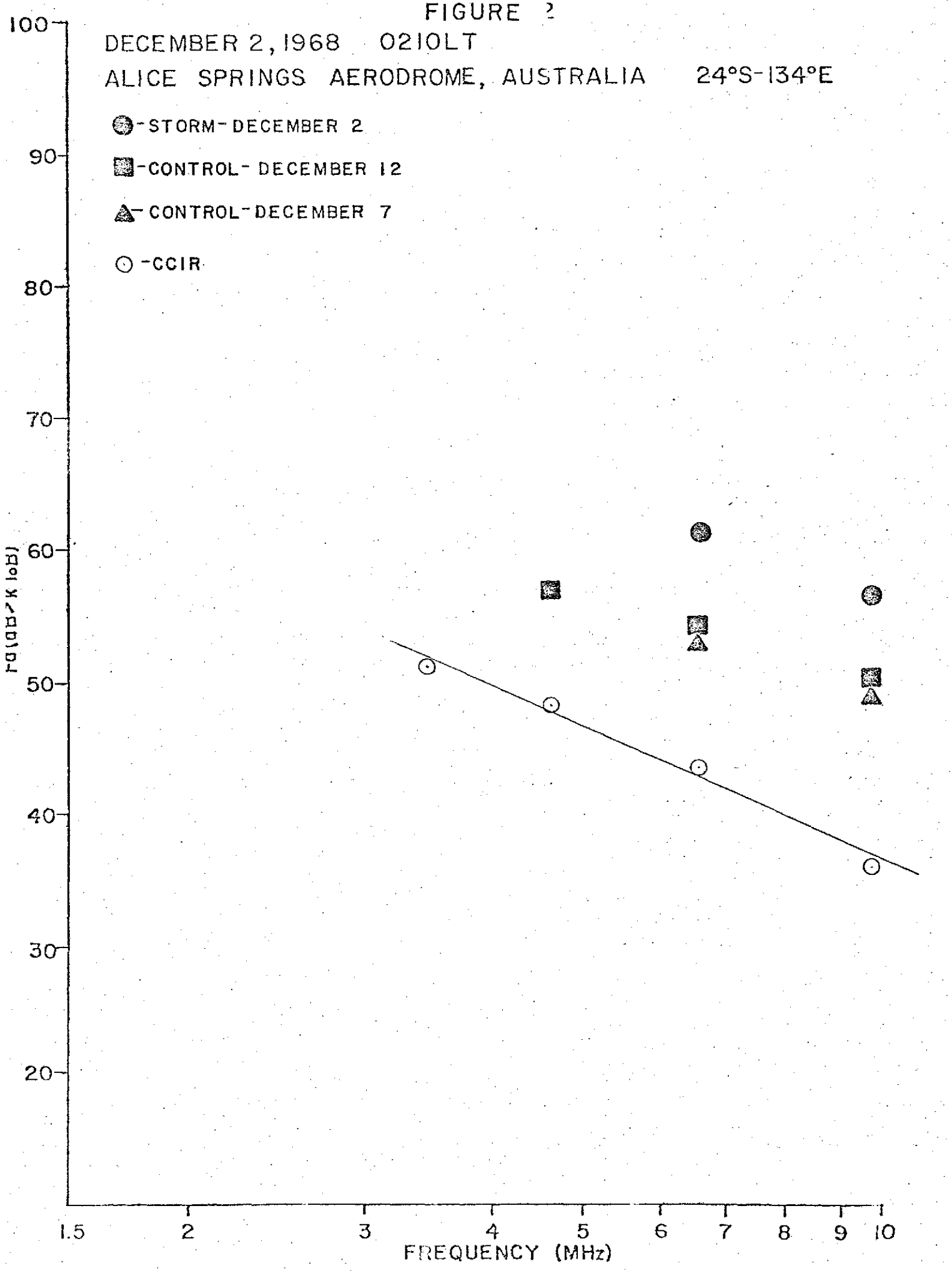
DECEMBER 2, 1968 0210LT
ALICE SPRINGS AERODROME, AUSTRALIA 24°S-134°E
-STORM- DECEMBER 2
-CONTROL- DECEMBER 12
-CONTROL- DECEMBER 7
-CCIR
100
90
80
70
60
50
40
30
20
Fa (dB above kTo B)
1.5
2
3
4
5
6
7
8
9
10
FREQUENCY (MHz)

FIGURE 3

AUGUST 21, 1969 0900 LT

CHARLEVILLE, AUSTRALIA 26°S-146°E

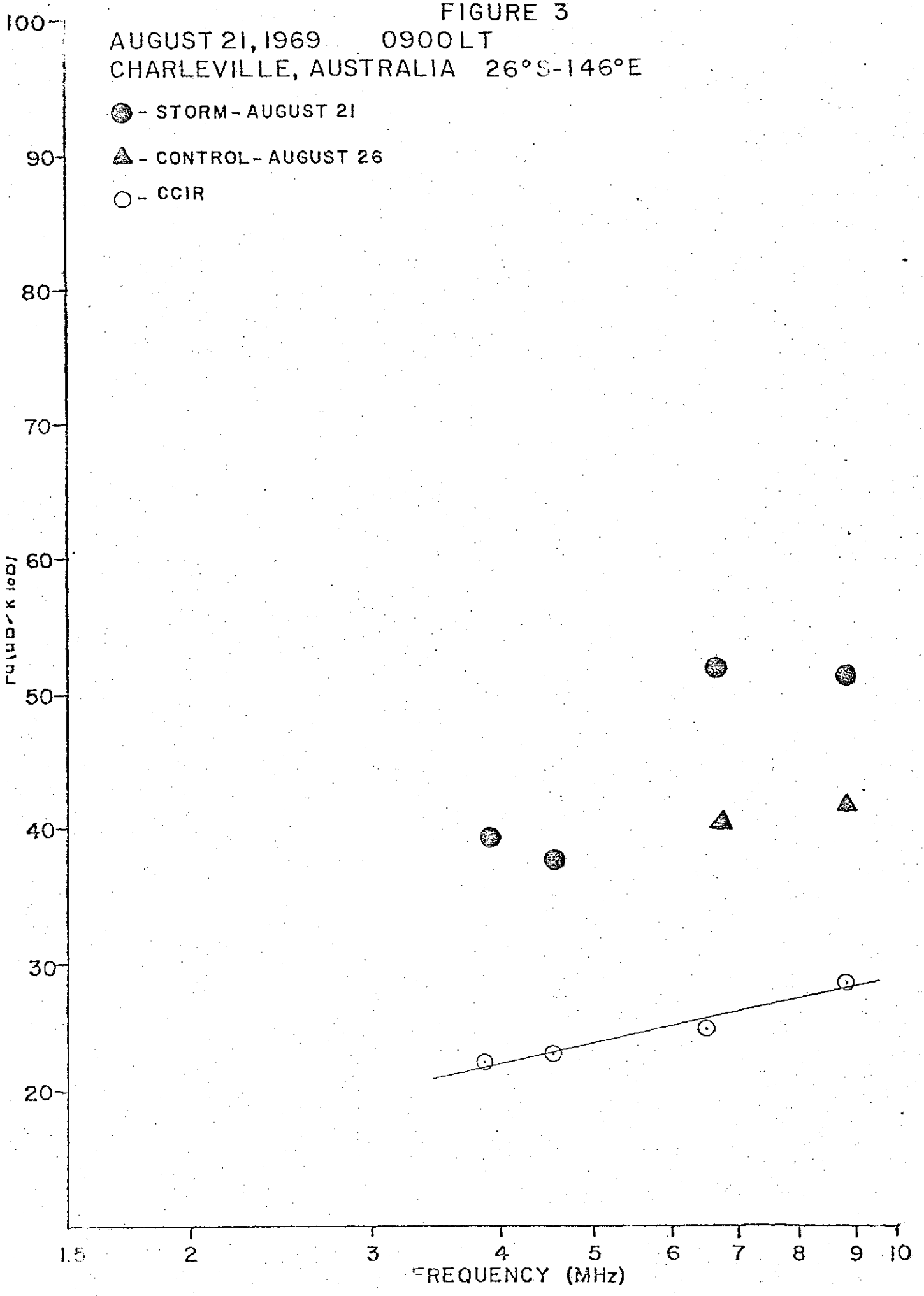

FIGURE 4

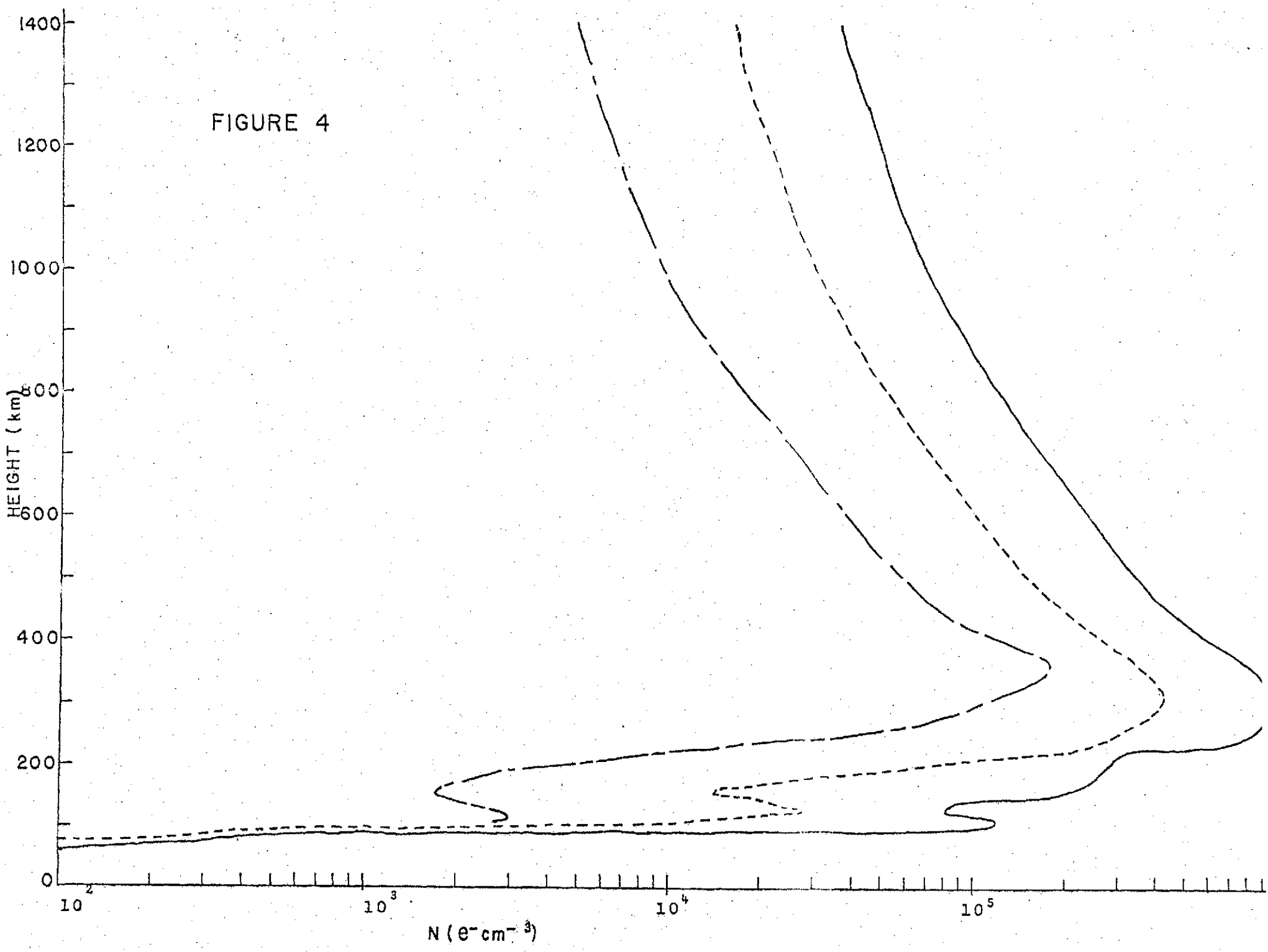
1400
1200
1000
800
600
400
200
0
HEIGHT (km)
10^2
10^3
10^4
10^5
N ($e^- cm^{-3}$)

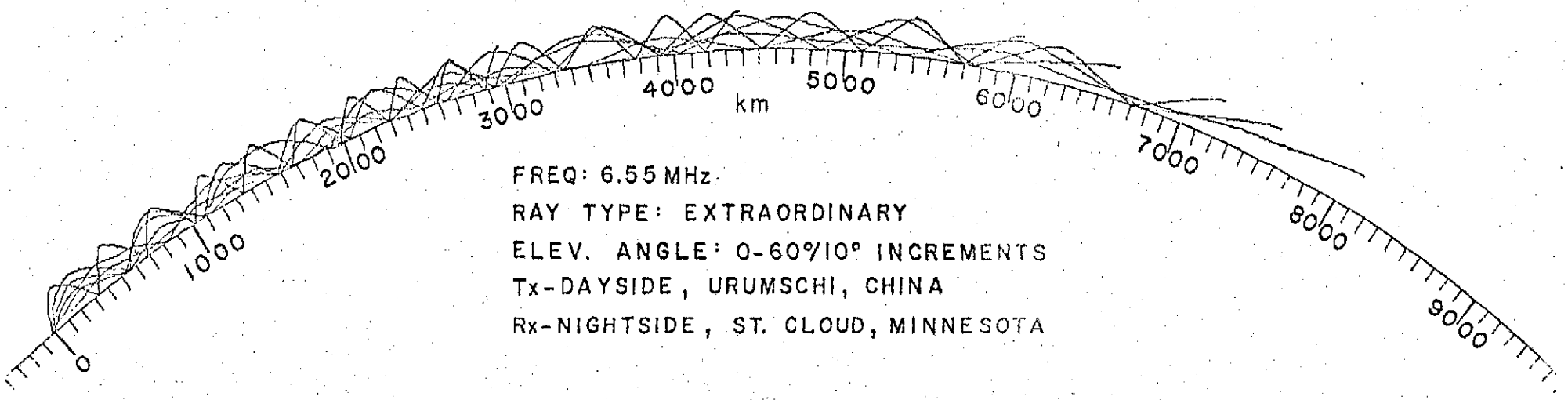
0
1000
2000
3000
4000
km
5000
6000
7000
8000
9000
FREQ: 6.55 MHz
RAY TYPE: EXTRAORDINARY
ELEV. ANGLE: 0-60°/10° INCREMENTS
Tx-DAYSIDE, URUMSCHI, CHINA
Rx-NIGHTSIDE, ST. CLOUD, MINNESOTA

FIGURE 5

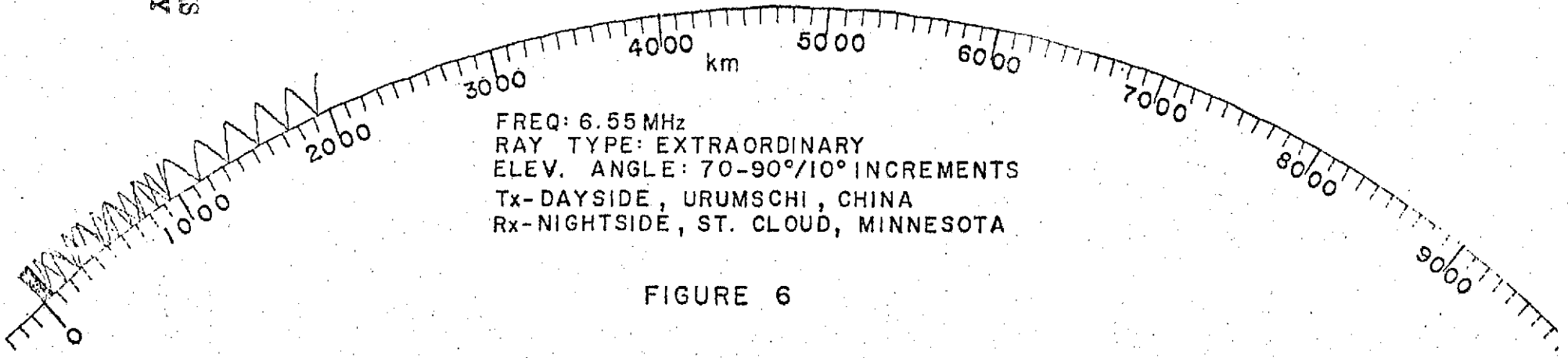

FIGURE 6

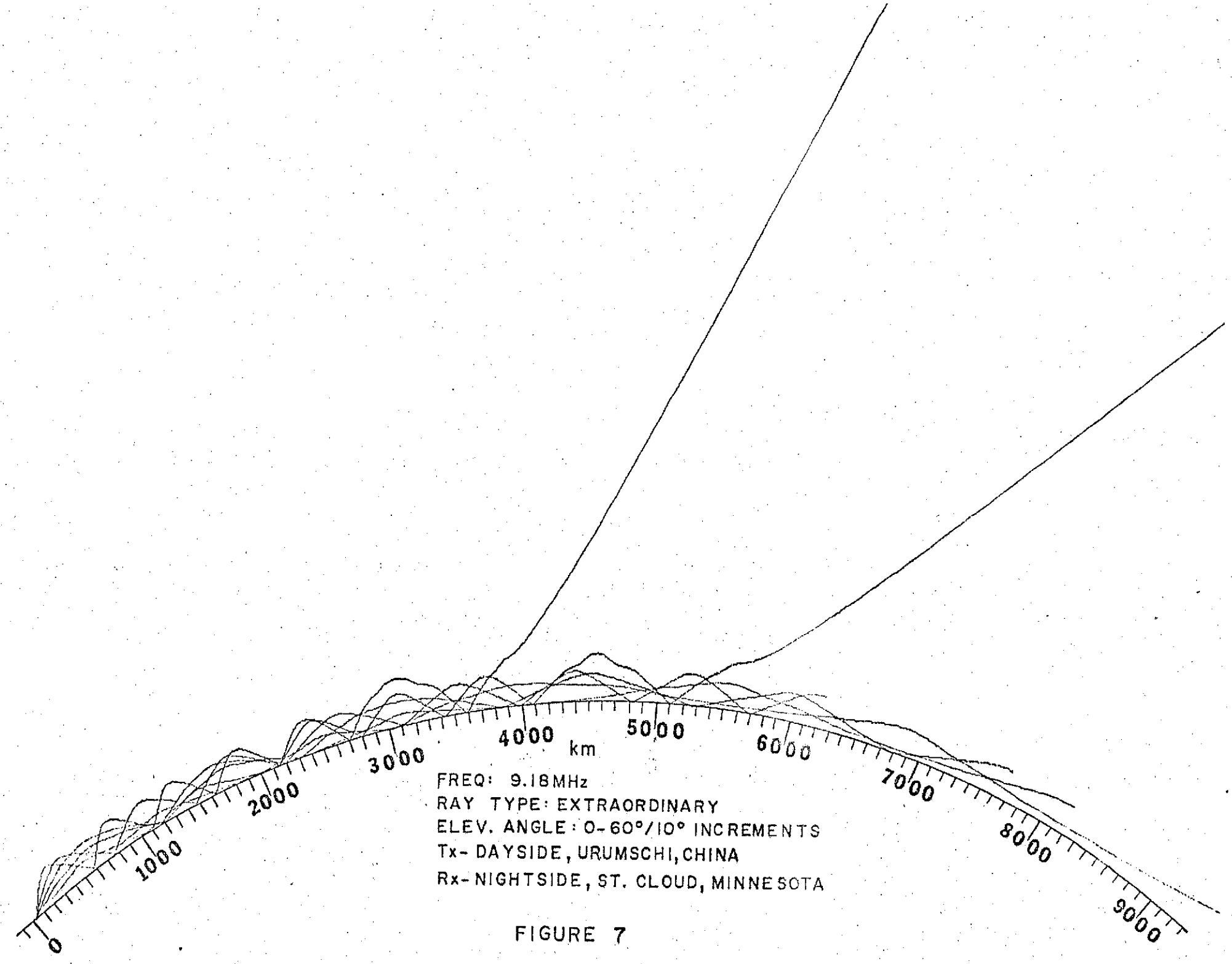
0
1000
2000
3000
4000
km
5000
6000
7000
8000
9000
FREQ: 9.18MHz
RAY TYPE: EXTRAORDINARY
ELEV. ANGLE: 0-60°/10° INCREMENTS
Tx- DAYSIDE, URUMSCHI, CHINA
Rx- NIGHTSIDE, ST. CLOUD, MINNESOTA

FIGURE 7

FIGURE 8

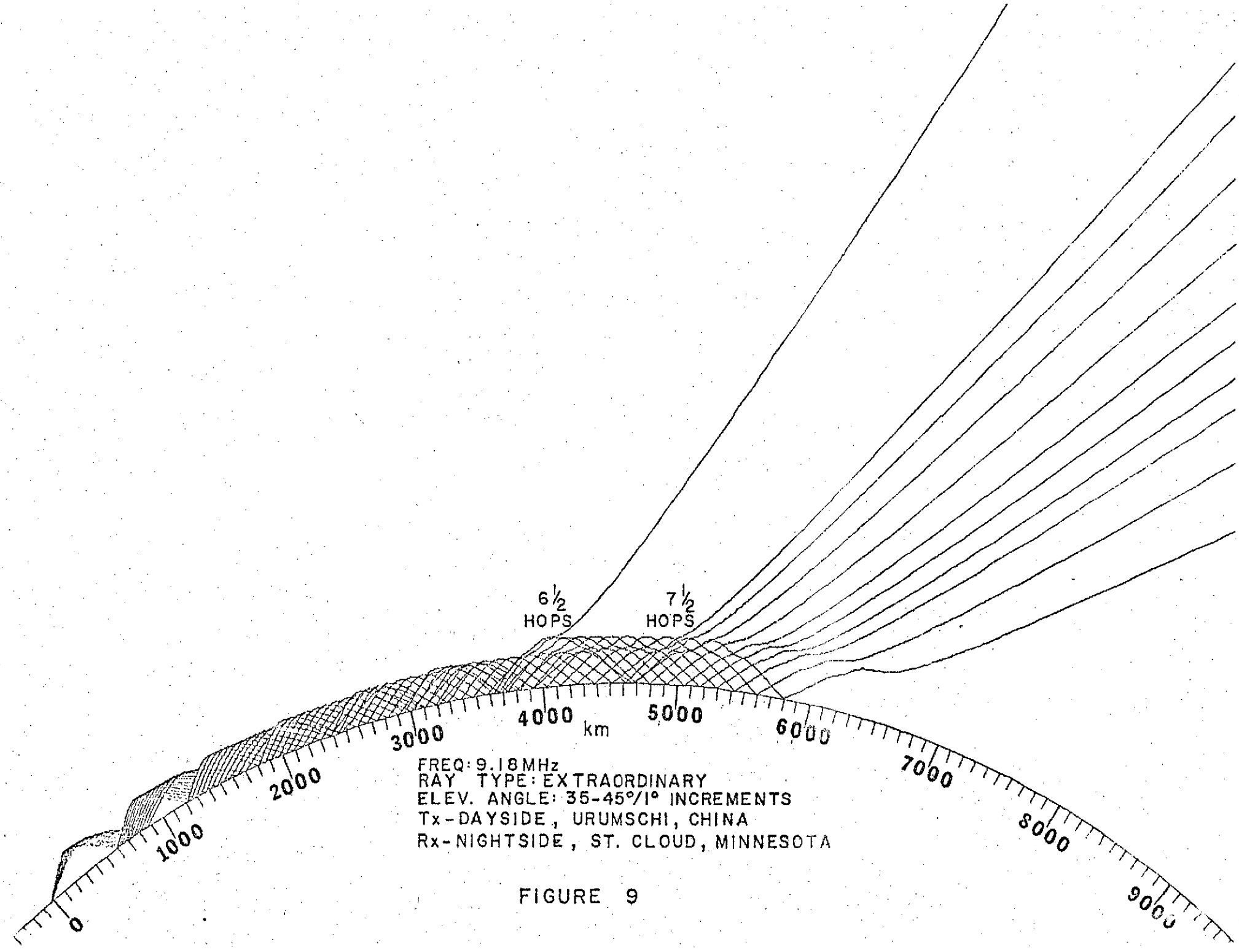
6½ HOPS
7½ HOPS
0
1000
2000
3000
4000
km
5000
6000
7000
8000
9000
FREQ: 9.18 MHz
RAY TYPE: EXTRAORDINARY
ELEV. ANGLE: 35-45°/1° INCREMENTS
Tx - DAYSIDE, URUMSCHI, CHINA
Rx - NIGHTSIDE, ST. CLOUD, MINNESOTA

FIGURE 9

FIGURE 10

15 SEPTEMBER 1969, 1740 UT

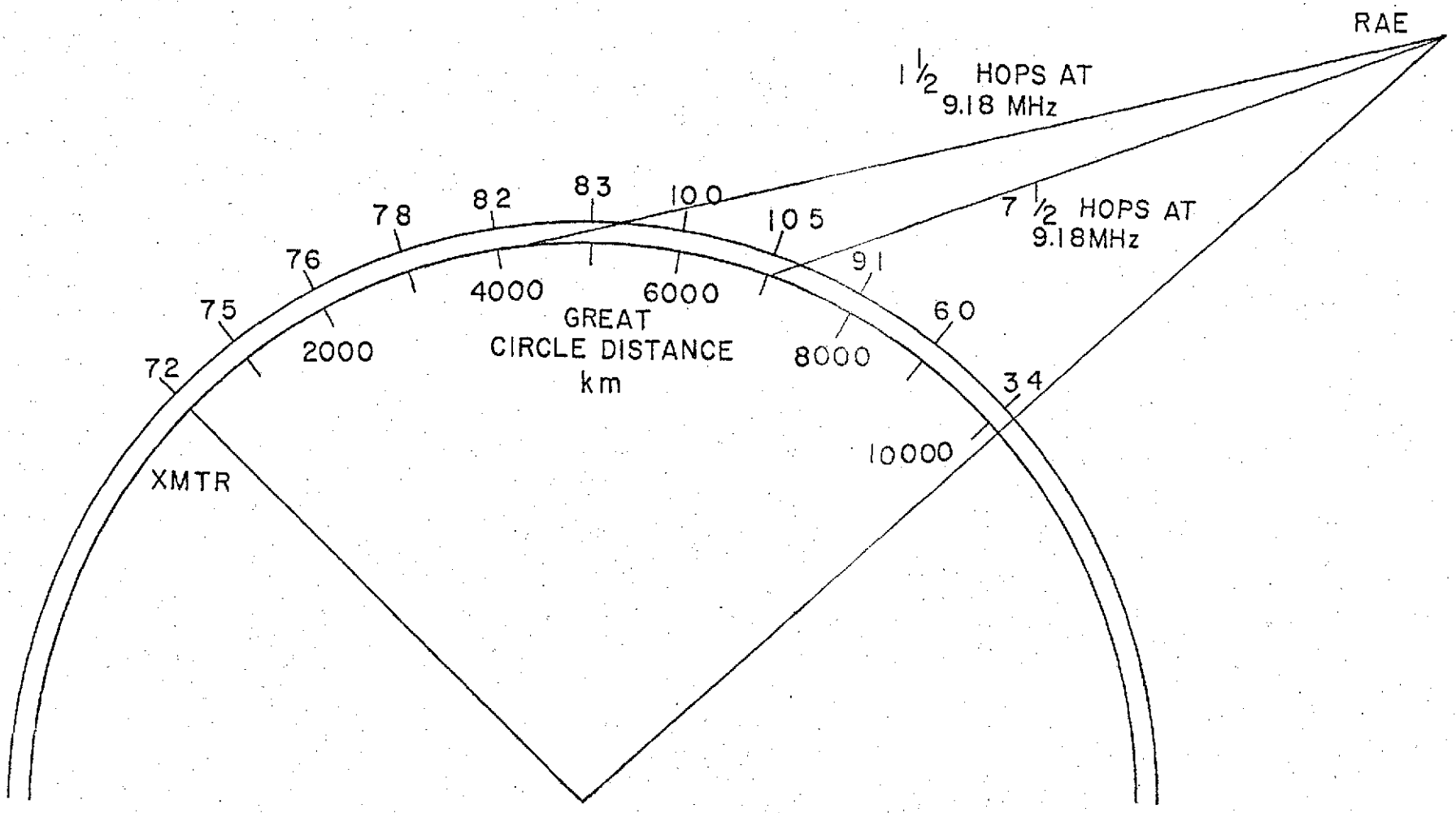

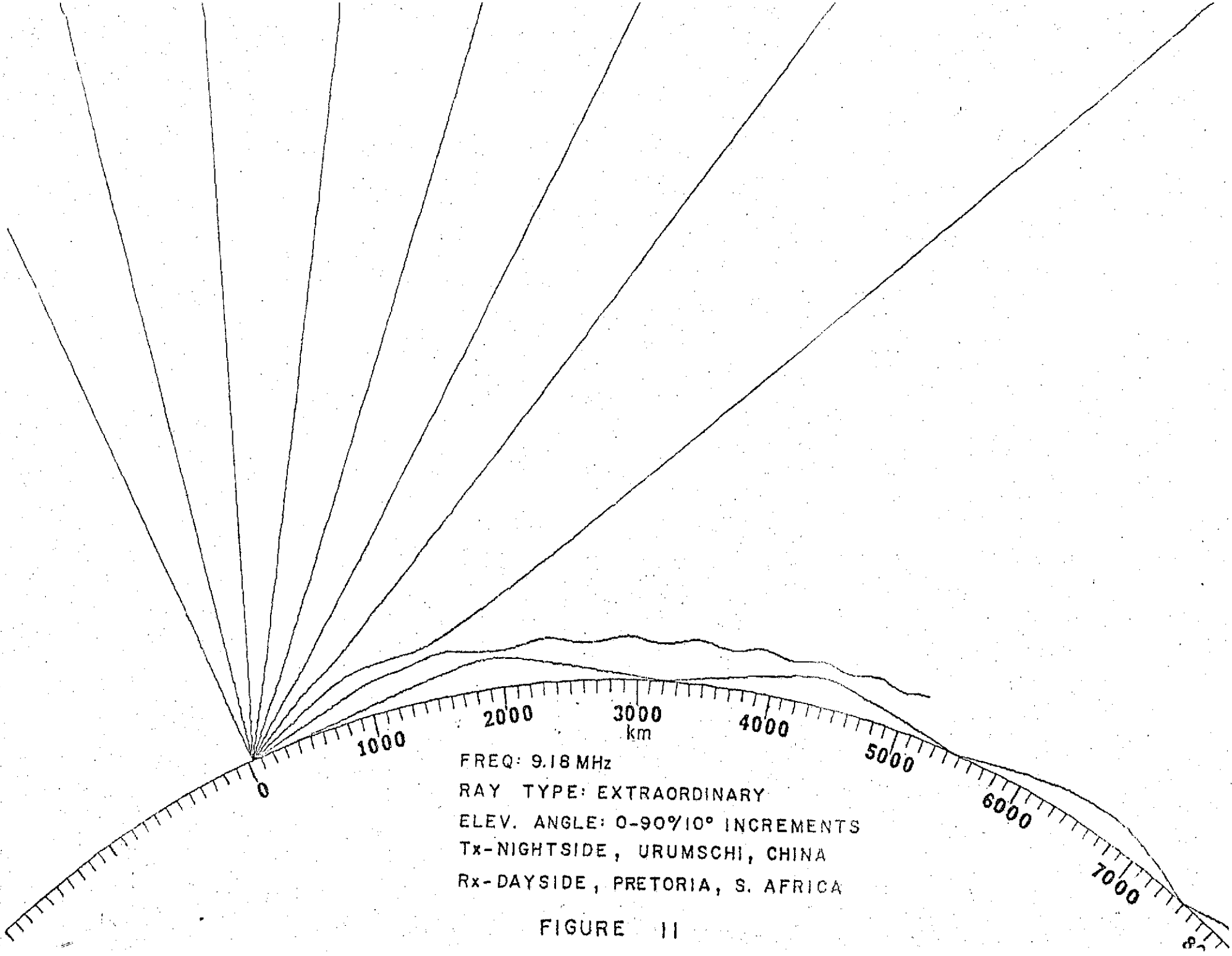
0
1000
2000
3000
km
4000
5000
6000
7000
FREQ: 9.18 MHz
RAY TYPE: EXTRAORDINARY
ELEV. ANGLE: 0-90°/10° INCREMENTS
Tx-NIGHTSIDE, URUMSCHI, CHINA
Rx-DAYSIDE, PRETORIA, S. AFRICA

FIGURE 11

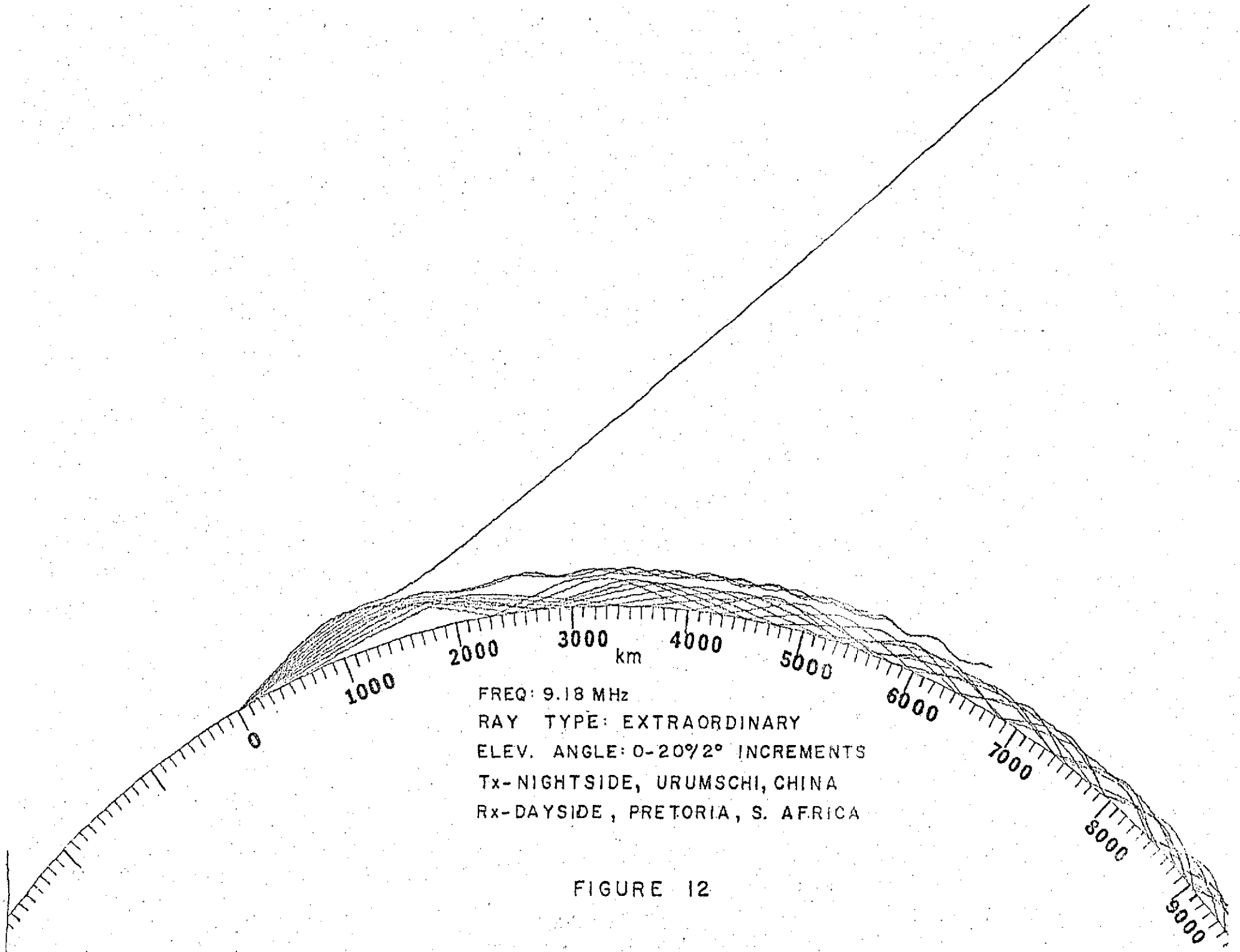
0
1000
2000
3000
km
4000
5000
6000
7000
8000
9000
FREQ: 9.18 MHz
RAY TYPE: EXTRAORDINARY
ELEV. ANGLE: 0-20%2° INCREMENTS
Tx-NIGHTSIDE, URUMSCHI, CHINA
Rx-DAYSIDE, PRETORIA, S. AFRICA

FIGURE 12

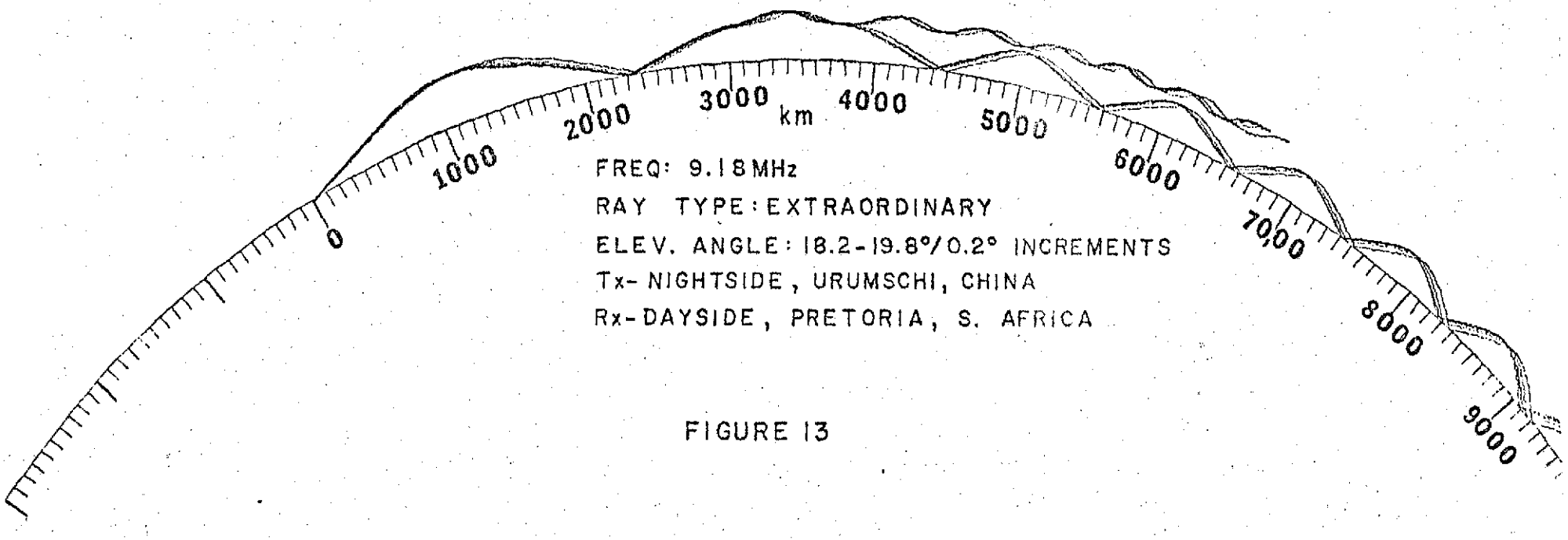
0
1000
2000
3000
km
4000
5000
6000
7000
8000
9000
FREQ: 9.18 MHz
RAY TYPE: EXTRAORDINARY
ELEV. ANGLE: 18.2-19.8°/0.2° INCREMENTS
Tx- NIGHTSIDE, URUMSCHI, CHINA
Rx- DAYSIDE, PRETORIA, S. AFRICA

FIGURE 13

FIGURE 14

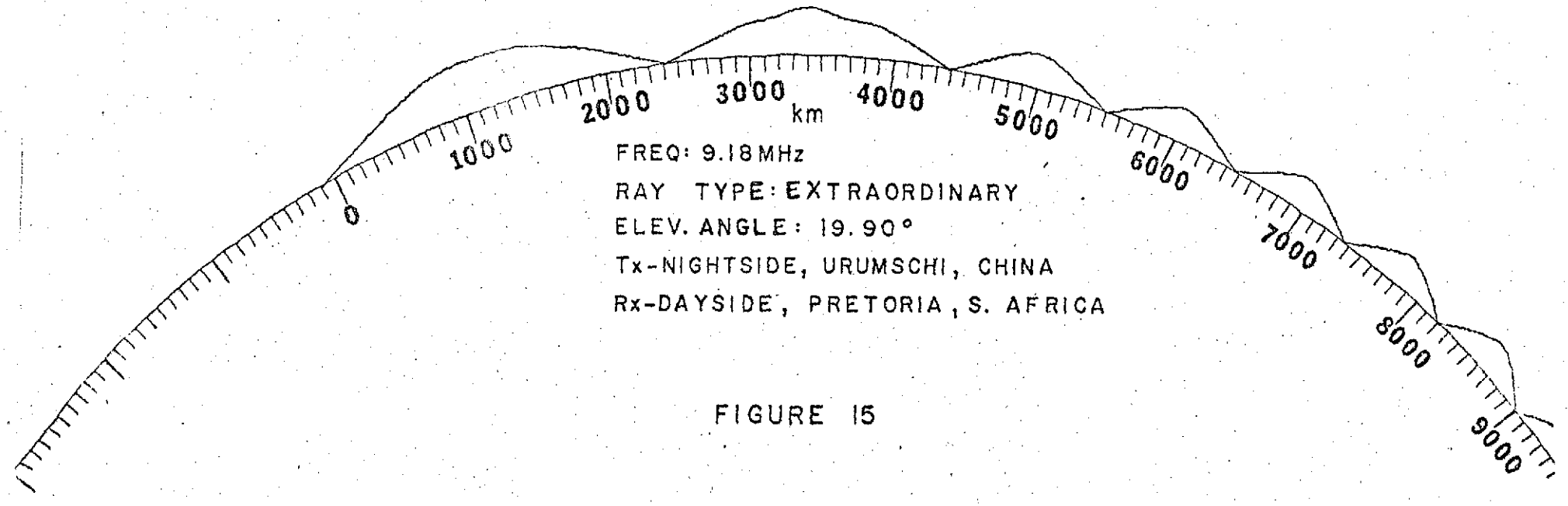
0
1000
2000
3000
km
4000
5000
6000
7000
8000
9000
FREQ: 9.18 MHz
RAY TYPE: EXTRAORDINARY
ELEV. ANGLE: 19.90°
Tx-NIGHTSIDE, URUMSCHI, CHINA
Rx-DAYSIDE, PRETORIA, S. AFRICA

FIGURE 15

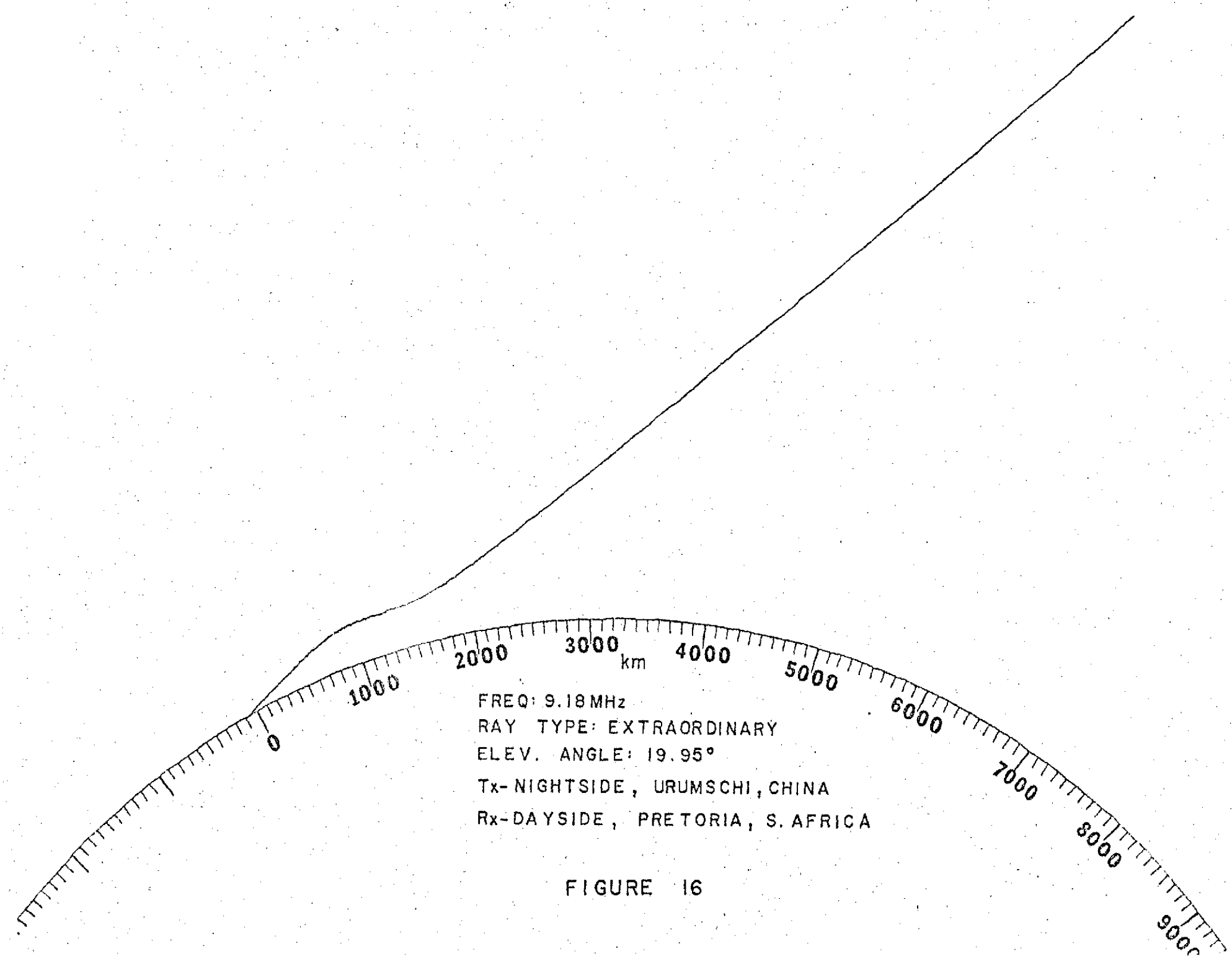
0
1000
2000
3000
km
4000
5000
6000
7000
8000
9000
FREQ: 9.18 MHz
RAY TYPE: EXTRAORDINARY
ELEV. ANGLE: 19.95°
Tx-NIGHTSIDE, URUMSCHI, CHINA
Rx-DAYSIDE, PRETORIA, S. AFRICA

FIGURE 16

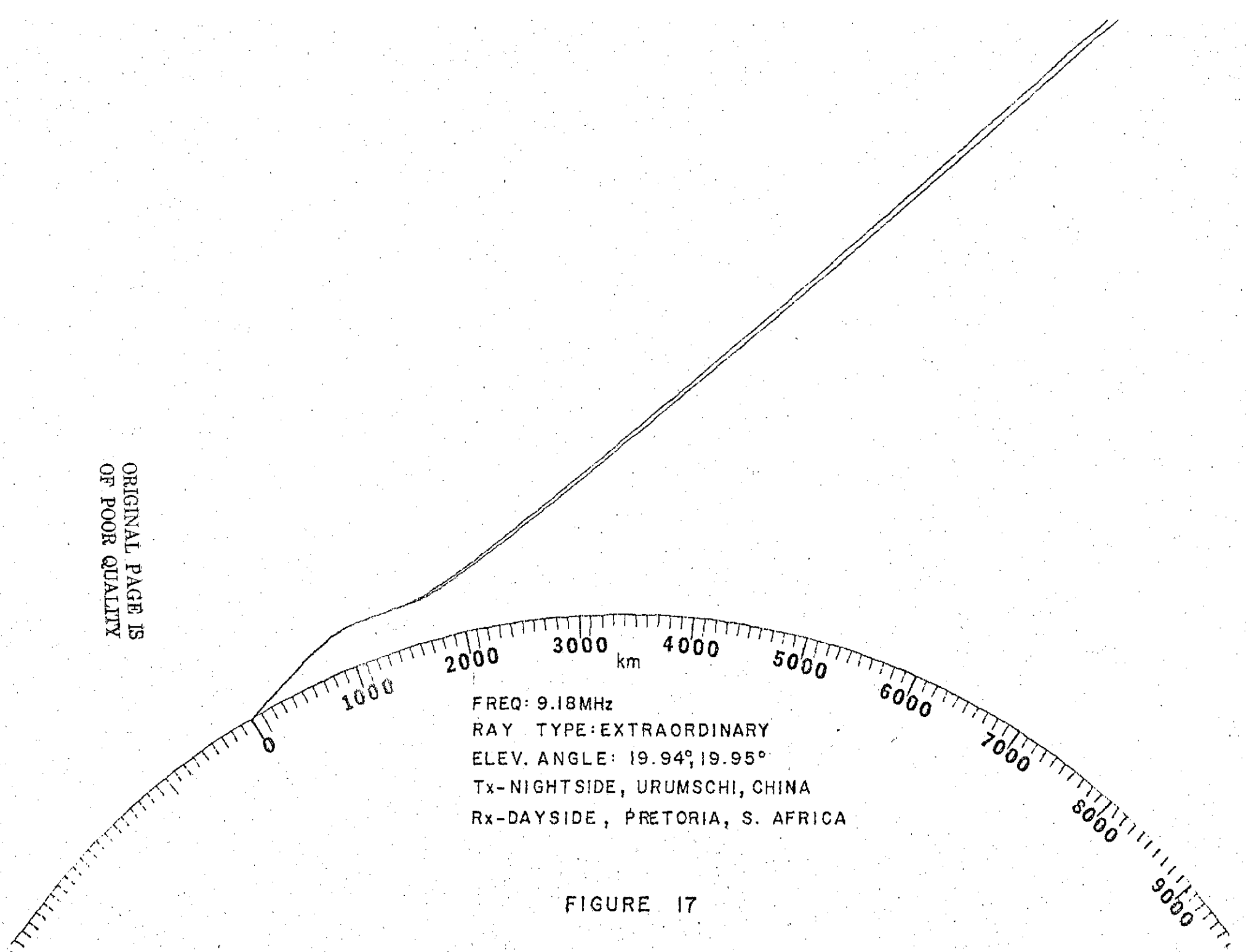

FIGURE 17

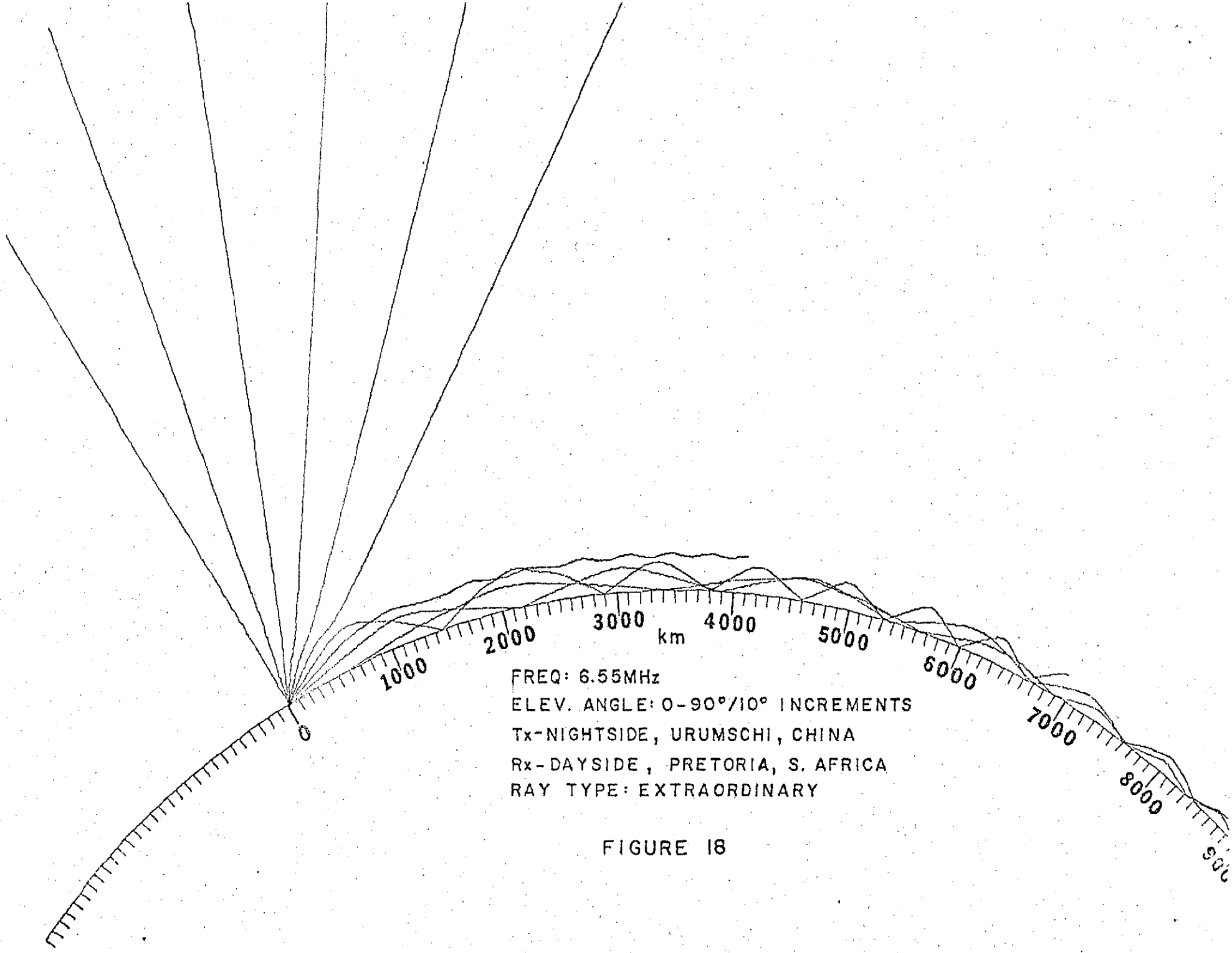
0
1000
2000
3000
km
4000
5000
6000
7000
8000
FREQ: 6.55MHz
ELEV. ANGLE: 0-90°/10° INCREMENTS
Tx-NIGHTSIDE, URUMSCHI, CHINA
Rx-DAYSIDE, PRETORIA, S. AFRICA
RAY TYPE: EXTRAORDINARY

FIGURE 18

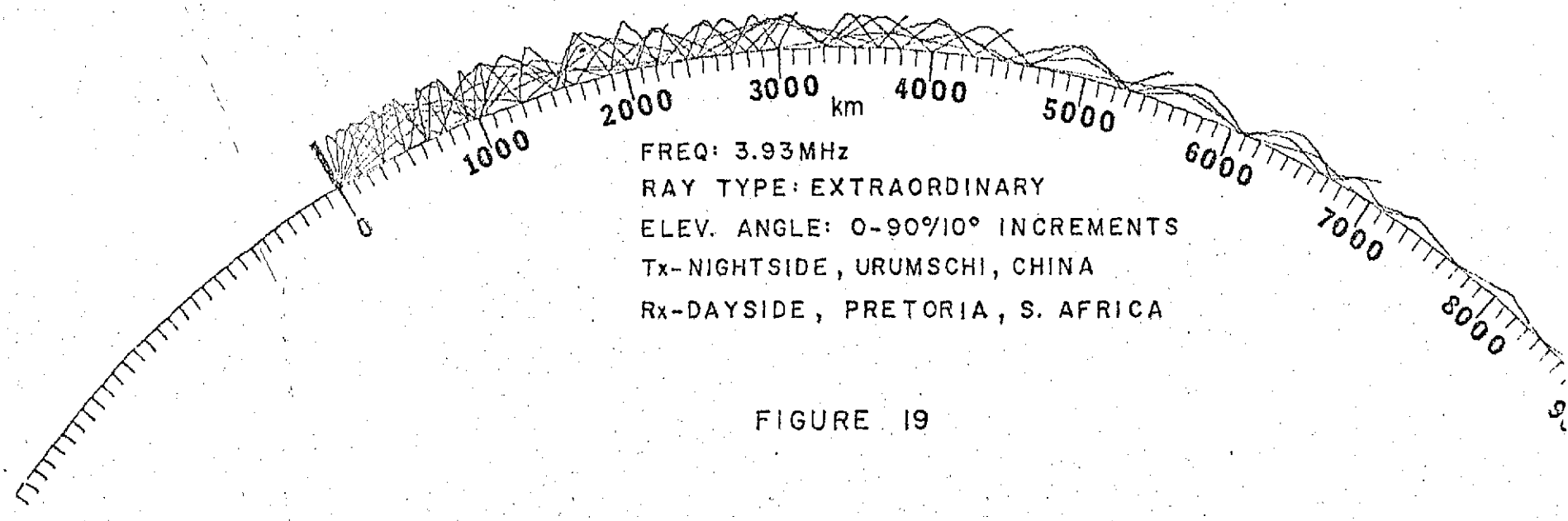
0
1000
2000
3000
km
4000
5000
6000
7000
8000
FREQ: 3.93MHz
RAY TYPE: EXTRAORDINARY
ELEV. ANGLE: 0-90°/10° INCREMENTS
Tx-NIGHTSIDE, URUMSCHI, CHINA
Rx-DAYSIDE, PRETORIA, S. AFRICA

FIGURE 19

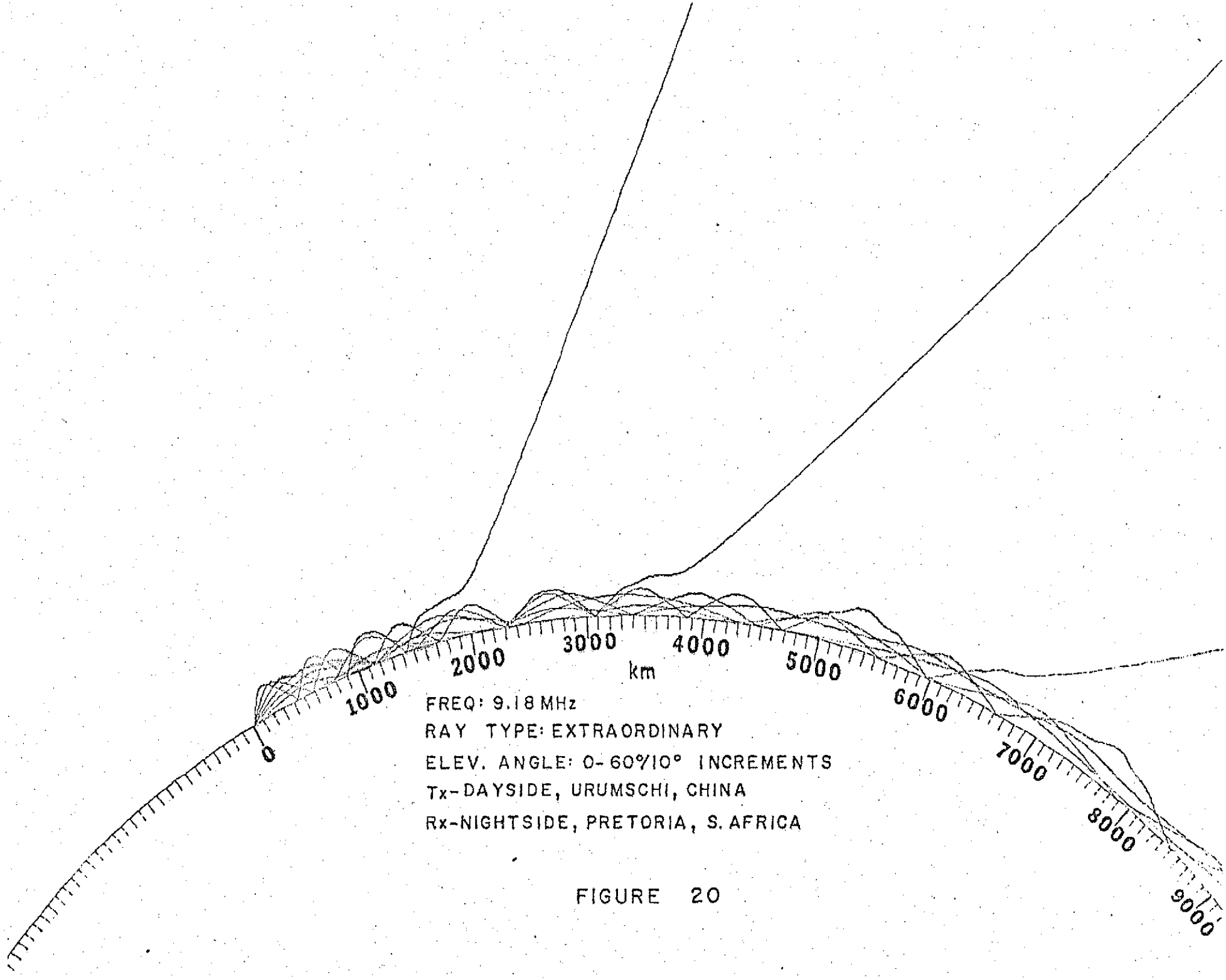
0
1000
2000
3000
4000
5000
6000
7000
8000
9000
km
FREQ: 9.18 MHz
RAY TYPE: EXTRAORDINARY
ELEV. ANGLE: 0-60%10° INCREMENTS
Tx-DAYSIDE, URUMSCHI, CHINA
Rx-NIGHTSIDE, PRETORIA, S. AFRICA

FIGURE 20

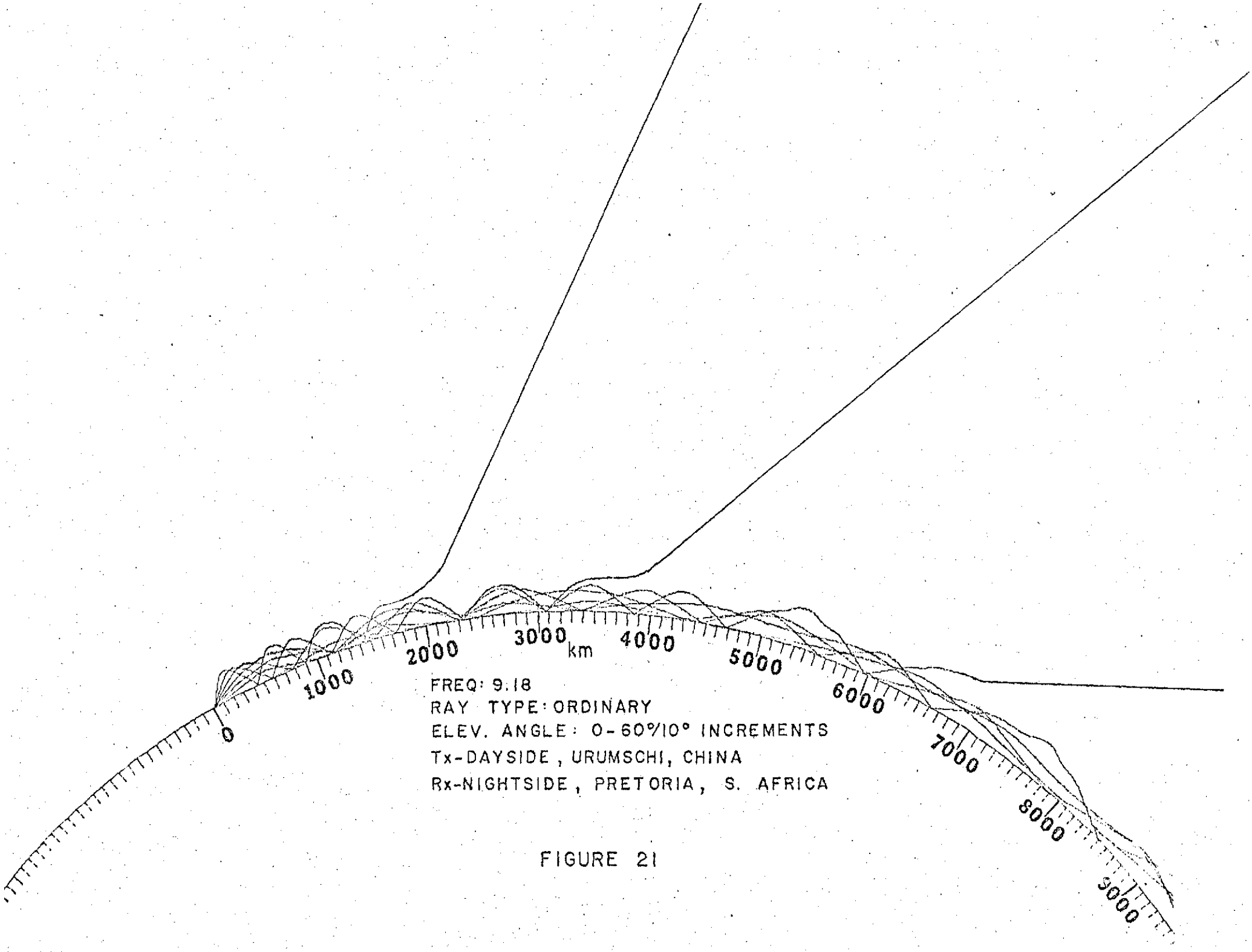
0
1000
2000
3000
km
4000
5000
6000
7000
8000
9000
FREQ: 9.18
RAY TYPE: ORDINARY
ELEV. ANGLE: 0-60°/10° INCREMENTS
Tx-DAYSIDE, URUMSCHI, CHINA
Rx-NIGHTSIDE, PRETORIA, S. AFRICA

FIGURE 21